

Critical temperatures of two dimensional magnets beyond linear spin wave theory: application to CrI_3 , MPS_3 (M=Ni, Mn, Fe) and CrSBr

Varun Rajeev Pavizhakumari¹ and Thomas Olsen^{1,*}

¹*Computational Atomic-Scale Materials Design (CAMD), Department of Physics, Technical University of Denmark, 2800 Kgs. Lyngby, Denmark*

Magnetic anisotropy is crucial for sustaining long range magnetic order in two-dimensional materials (2D) and must be taken into account by any approximate scheme for calculating critical temperatures. While 2D ferromagnets have received significant attention with regard to predicting Curie temperatures, the treatment of 2D anti-ferromagnetism has largely been restricted to classical approaches, which typically underestimate Néel temperatures. The concept of anti-ferromagnetism can be regarded as a special case of single- Q magnetic order, and for such systems the critical temperature can be calculated from the magnon dispersion using either Holstein-Primakoff (HP) bosonization or Green's function-based Random Phase Approximation (RPA). Here, we study the effects of single-ion anisotropy in general single- Q systems in both the HP and RPA methods. In the case of RPA, we generalize the approach to include the Callen Decoupling (CD) correction, which has previously been shown to yield good agreement with experimental Curie temperatures for 2D ferromagnets. We compare the calculated critical temperatures of CrI_3 (uniaxial ferromagnet), MPS_3 (M=Ni, Mn, Fe) (uniaxial anti-ferromagnets) and CrSBr (triaxial ferromagnet) monolayers with experimental values and find that the Green's function-based methods are much more reliable than HP and that the CD decoupling appears to be more accurate than RPA if the single-ion anisotropy is large.

I. INTRODUCTION

Since the discovery of ferromagnetic order in monolayer CrI_3 [1] there has been an increasing interest in magnetic two-dimensional materials. In addition to the fundamental physical aspects associated with two-dimensional (2D) magnetism, a wide variety of possible spintronics applications have been proposed [2, 3]. Compared to three-dimensional (3D) magnetic materials, a major difference is the crucial role played by magnetic anisotropy. The Mermin-Wagner (MW) theorem states that continuous symmetries cannot be *spontaneously* broken at finite temperature in 2D systems with short-range interactions [4] and this implies that order requires *explicit* symmetry breaking by magnetic anisotropy. While one may still obtain a reliable description of the magnetic interactions in terms of Heisenberg models, well-established methodology for calculating magnetic properties of such models may break down in 2D. For example, conventional Weiss mean field theory predicts a finite critical temperature in any isotropic model - irrespective of the dimensionality of the lattice - and thus fails rather dramatically in 2D. On the other hand, correlation effects can be accounted for by applying classical Monte Carlo (MC) simulations, which are commonly used to estimate critical temperatures [5–8]. However, such calculations are often computationally demanding and accuracy is typically limited by the classical treatment [9]. Finally, one may try to obtain the thermal properties directly from the quantum mechanical excitations, which can be calculated by various approximate

methods. In the case of long range order, the fundamental magnetic excitations of the Heisenberg model will be comprised by magnons, and while single-magnon energies are easily calculated, magnon-magnon interactions have to be approximated at the mean-field level. This leads to a temperature-dependent renormalization of magnon energies, which can be calculated in either the Holstein Primakoff (HP) bosonization scheme or in the Green's function-based Random Phase Approximation (RPA) [10–12]. These methods have recently been developed and benchmarked against experimental critical temperatures in 3D materials [9], but due to the importance of magnetic anisotropy in 2D, the application to 2D magnetism calls for a study of its own.

At the level of two-spin interactions, spin-orbit coupling may give rise to either anisotropic exchange (two-site) interactions or single-ion (one-site) anisotropy. The former case can be handled rather generally by introducing an exchange tensor describing the magnetic interaction between two sites and is straightforward to include in both HP [13] and RPA [9]. The single-ion anisotropy may be included in these approaches as well, but the associated mean-field approximation becomes much more subtle because the two spin operators do not commute at the same site. For example, the generalized single- Q method of Ref. [9], can handle uniaxial, biaxial and triaxial single-ion anisotropies in the Heisenberg model, but RPA fails to predict the irrelevance of single-ion anisotropy for the case of $S = 1/2$ systems. The HP method (with a mean-field treatment of two-magnon interactions) correctly captures the vanishing spin-wave gap (irrelevance of single-ion anisotropy) for uniaxial ferromagnets at $T = 0$, but fails to do so at elevated temperatures as well as tri-axial systems at $T = 0$. An alternative to RPA was proposed by Herbert Callen in 1963

* tolsen@fysik.dtu.dk

[14] and will be referred to as Callen Decoupling (CD) in the following. Callen's scheme comprises an alternative mean-field decoupling of the equation of motion, which may be applied to the calculations of critical temperatures. We have recently shown that in this respect the method performs better than RPA in the classical limit (relevant for itinerant systems), but not in the quantum regime [15]. However, CD gives the correct behavior for the single-ion anisotropy contribution to the magnon dispersion (irrelevance of single-ion anisotropy and vanishing spin-wave gap for $S = 1/2$ systems), and it has been shown that augmenting the RPA method for exchange interactions with CD for the single-ion anisotropy (RPA+CD) gives excellent agreement with exact results for ferromagnets [15, 16]. The CD has been developed for simple anti-ferromagnets [17, 18] as well, but a general approach for arbitrary single- Q states seems to be lacking in the literature.

In this work, we conduct a systematic study of the effect of single-ion anisotropy on the prediction of critical temperature obtained by various approximations. The methods are applied to well-known 2D magnets that represent different types of order: CrI_3 (uniaxial ferromagnet), MPS_3 ($M=\text{Ni, Mn, Fe}$) (uniaxial anti-ferromagnets) and CrSBr (triaxial ferromagnet). We use the experimental exchange constants obtained from inelastic neutron scattering experiments and compare the critical temperatures calculated with HP, RPA, RPA+CD and classical MC with experimental values.

The paper is organized as follows. In sec. II A, we generalize the HP method to include a mean-field description of magnon-magnon interactions for arbitrary single- Q states. In sec. II B, we include the single-ion anisotropy tensor in both the RPA and the CD approach for single- Q ordered systems. Sec. II C, details the behavior of 2D critical temperatures as the single-ion anisotropy approaches zero and Sec. II D generalizes the theory to include dipole-dipole interactions. Finally, in sec. III, we calculate the critical temperature of CrI_3 , MPS_3 ($M=\text{Ni, Mn, Fe}$) and CrSBr and compare the performance of the different methods.

II. THEORY

Our starting point is the Heisenberg model

$$\mathcal{H} = -\frac{1}{2} \sum_{abij} \mathbf{S}_{ai}^T \mathbf{J}_{abij} \mathbf{S}_{bj} \quad (1)$$

where \mathbf{S}_{ai} is the spin operator for site a in unit cell i and \mathbf{J}_{abij} is the exchange tensor that couples spins at i, a and j, b . Written in this form the model includes single-ion anisotropy represented by the terms with $a = b$ and $i = j$. In the following it will be practical to consider such terms separately and we write them as

$$\mathcal{H}_K = - \sum_{ai} \mathbf{S}_{ai}^T \mathbf{K}_{ai} \mathbf{S}_{ai}, \quad (2)$$

with $\mathbf{K}_{ai} = \mathbf{J}_{aaii}/2$ being the single-ion anisotropy tensor. It should be noted that the magnon dispersion must be invariant under the addition of an isotropic term to the single-ion anisotropy tensor: $\mathbf{K}_{ai}^{\mu\nu} \rightarrow \mathbf{K}_{ai}^{\mu\nu} + \alpha \delta^{\mu\nu}$. This is due to the fact that $\mathbf{S}_{ai} \cdot \mathbf{S}_{ai}$ is a constant and will be referred to as isotropic invariance. This freedom will be utilized to enforce certain components of the tensor to vanish in the following. It is also clear that the single-ion anisotropy term becomes a constant (and thus irrelevant) for any $S = 1/2$ system.

In the present work we focus on a rather general type of magnetic order referred to as single- Q states. For such cases the ground state magnetic structure is characterized by an ordering vector \mathbf{Q} , a global rotation axis $\hat{\mathbf{n}}$ and the relative direction of the magnetic moments in a particular unit cell. The spins in different unit cells are then related by $\langle \mathbf{S}_{ai} \rangle = \mathbf{R}_{\hat{\mathbf{n}}}(\mathbf{Q} \cdot \mathbf{r}_{ij}) \langle \mathbf{S}_{aj} \rangle$, where $\mathbf{R}_{\hat{\mathbf{n}}}$ is a rotation matrix and \mathbf{r}_{ij} is a lattice vector connecting cell i to cell j . It will be convenient to transform the system to a local coordinate system where all spin fluctuations are perpendicular to the local- z axis. This entails a rotation of all spin operators into a locally ferromagnetic system and can be divided into two steps: a cell-dependent rotation \mathbf{R}_i and a site-dependent (cell-independent) rotation \mathbf{R}'_a . The spin operators are then written as

$$\mathbf{S}_{ai} = \mathbf{R}_i \mathbf{S}'_{ai}, \quad (3)$$

$$\mathbf{R}_i = \mathbf{R}_{\hat{\mathbf{n}}}(\mathbf{Q} \cdot \mathbf{r}_i), \quad (4)$$

$$\mathbf{S}'_{ai} = \mathbf{R}'_a \mathbf{S}''_{ai}, \quad (5)$$

where $\hat{\mathbf{n}}$ is the global rotation axis for the single- Q spiral state, \mathbf{S}'_{ai} are spins in the coordinates that are independent of unit cells and \mathbf{S}''_{ai} are spins in the locally ferromagnetic frame independent of sites [9, 13]. Introducing two new vectors \mathbf{u}_a and \mathbf{v}_a

$$[\mathbf{u}_a]^\mu = [\mathbf{R}'_a]^\mu{}^x + i [\mathbf{R}'_a]^\mu{}^y, \quad (6)$$

$$[\mathbf{v}_a]^\mu = [\mathbf{R}'_a]^\mu{}^z. \quad (7)$$

Eq. (2) can be written as

$$\mathcal{H}_K = - \sum_{ai} \mathbf{S}_{ai}^T \mathbf{K}_a \mathbf{S}'_{ai}, \quad (8)$$

where

$$\mathbf{S}'_{ai} = \mathbf{u}_a \frac{S_{ai}^{\prime\prime+}}{2} + \mathbf{u}_a^* \frac{S_{ai}^{\prime\prime-}}{2} + \mathbf{v}_a S_{ai}^{\prime\prime z}. \quad (9)$$

and we used the rotational symmetry of the anisotropy tensor, which implies $\mathbf{R}_i^T \mathbf{K}_{ai} \mathbf{R}_i = \mathbf{K}_{ai} = \mathbf{K}_a$.

Before we proceed we note that the presence of single-ion anisotropy may or may not be consistent with the assumption of a single- Q state. For example, the well-known case of a 2D hexagonal lattice with nearest neighbor anti-ferromagnetic isotropic interactions, gives rise to a ground state with 120° between all spins. This is a planar spin spiral, which can be described as a single- Q state with $\mathbf{Q} = (1/3, 1/3)$. If single-ion anisotropy

is included, symmetry dictates that it must be uniaxial, which implies an easy-plane or an easy-axis. In the former case, the spiral plane coincides with the lattice plane and the single- Q structure is preserved. However, for easy-axis anisotropy the spiral plane becomes orthogonal to the lattice and the 120° symmetry will be slightly (if anisotropy is small) broken. The compatibility of a given single- Q state (including orientation) with a single-ion anisotropy tensor is essentially captured by whether or not the condition $\mathbf{R}_i^T \mathbf{K}_{ai} \mathbf{R}_i = \mathbf{K}_{ai}$ is satisfied.

A. Holstein-Primakoff bosonization

In the HP approach we express the spin operators in terms of bosonic operators, which ensure that the commutators between spin operators are conserved. In the local reference frame, the ground state spin direction is always along z and we thus apply the *local* Holstein-Primakoff transformation [10, 13],

$$S_{ai}^{\prime\prime+} = \sqrt{2S_a} \sqrt{1 - \frac{a_{ai}^\dagger a_{ai}}{2S_a}} a_{ai}, \quad (10)$$

$$S_{ai}^{\prime\prime-} = \sqrt{2S_a} a_{ai}^\dagger \sqrt{1 - \frac{a_{ai}^\dagger a_{ai}}{2S_a}}, \quad (11)$$

$$S_{ai}^{\prime\prime z} = S_a - a_{ai}^\dagger a_{ai}, \quad (12)$$

where S_a is the maximum eigenvalue of the spin operator at sublattice a . Applying this to Eq. (9), and truncating the square roots at third order in bosonic operators we obtain

$$\begin{aligned} \mathbf{S}'_{ai} &\approx \mathbf{u}_a^{*T} \left(\sqrt{\frac{S_a}{2}} a_{ai} - \frac{a_{ai}^\dagger a_{ai} a_{ai}}{4\sqrt{2S_a}} \right) \\ &+ \mathbf{u}_a^T \left(\sqrt{\frac{S_a}{2}} a_{ai}^\dagger - \frac{a_{ai}^\dagger a_{ai}^\dagger a_{ai}}{4\sqrt{2S_a}} \right) \\ &+ \mathbf{v}_a^T (S_a - a_{ai}^\dagger a_{ai}). \end{aligned} \quad (13)$$

Using this, the Hamiltonian (8) can be expanded up to fourth order in bosonic operators:

$$\mathcal{H}_K \approx \mathcal{E}_K^0 + \mathcal{H}_K^2 + \mathcal{H}_K^4, \quad (14)$$

where

$$\mathcal{E}_K^0 = -N \sum_a (\mathbf{v}_a^T \mathbf{K}_a \mathbf{v}_a S_a (S_a + 1)), \quad (15)$$

$$\begin{aligned} \mathcal{H}_K^2 &= \sum_{ai} \left(S_a \mathbf{v}_a^T \mathbf{K}_a \mathbf{v}_a (a_{ai}^\dagger a_{ai} + a_{ai} a_{ai}^\dagger) \right. \\ &\quad \left. - \frac{S_a}{2} (\mathbf{u}_a^{*T} \mathbf{K}_a \mathbf{u}_a^* a_{ai} a_{ai} + \mathbf{u}_a^{*T} \mathbf{K}_a \mathbf{u}_a a_{ai} a_{ai}^\dagger \right. \\ &\quad \left. + \mathbf{u}_a^T \mathbf{K}_a \mathbf{u}_a^* a_{ai}^\dagger a_{ai} + \mathbf{u}_a^T \mathbf{K}_a \mathbf{u}_a a_{ai}^\dagger a_{ai}^\dagger) \right), \end{aligned} \quad (16)$$

$$\begin{aligned} \mathcal{H}_K^4 &= \sum_{ai} \left(-\mathbf{v}_a^T \mathbf{K}_a \mathbf{v}_a a_{ai}^\dagger a_{ai} a_{ai}^\dagger a_{ai} \right. \\ &\quad \left. + \frac{1}{8} (\mathbf{u}_a^{*T} \mathbf{K}_a \mathbf{u}_a^* (2a_{ai}^\dagger a_{ai} a_{ai} a_{ai} + a_{ai} a_{ai}) \right. \\ &\quad \left. + \mathbf{u}_a^{*T} \mathbf{K}_a \mathbf{u}_a (2a_{ai} a_{ai} a_{ai}^\dagger a_{ai}^\dagger) \right. \\ &\quad \left. + \mathbf{u}_a^T \mathbf{K}_a \mathbf{u}_a^* 2a_{ai}^\dagger a_{ai}^\dagger a_{ai} a_{ai} \right. \\ &\quad \left. + \mathbf{u}_a^T \mathbf{K}_a \mathbf{u}_a (2a_{ai}^\dagger a_{ai}^\dagger a_{ai}^\dagger a_{ai} + a_{ai}^\dagger a_{ai}^\dagger) \right), \end{aligned} \quad (17)$$

where N is the number of unit cells. We note that normal ordering of the quartic terms generates more quadratic terms that were not taken into account in \mathcal{H}_K^2 and will affect the zero-temperature dispersion. The bosonic operators are then Fourier transformed:

$$a_{a,\mathbf{q}} = \frac{1}{\sqrt{N}} \sum_i a_{ai} e^{i\mathbf{q}\cdot\mathbf{r}_i}, \quad a \in [1, N_a], \quad (18)$$

which results in fourth order terms like $a_{a,\mathbf{q}}^\dagger a_{a,\mathbf{q}'}^\dagger a_{a,\mathbf{q}''} a_{a,\mathbf{q}+\mathbf{q}'-\mathbf{q}''}$. These are subjected to a mean field decoupling leading to terms of the form $a_{a,\mathbf{q}}^\dagger a_{a,\mathbf{q}} \langle a_{a,\mathbf{q}'}^\dagger a_{a,\mathbf{q}'} \rangle \delta_{\mathbf{q},\mathbf{q}''}$, where $\langle \dots \rangle$ denotes the thermal average, which is assumed to vanish unless the bosonic operators contain the same wavevectors. Introducing the vector

$$\mathbf{a}_{\mathbf{q}} = \left[a_{a,\mathbf{q}} \quad a_{b,-\mathbf{q}}^\dagger \right]^T, \quad a, b \in [1, N_a], \quad (19)$$

Eq. (8) can be expressed as

$$\mathcal{H} = \mathcal{E}_0 + \mathcal{E}_K^0 + \sum_{\mathbf{q}} \mathbf{a}_{\mathbf{q}}^\dagger (\mathbf{H}_{\mathbf{q}}^{\text{HP}} + \mathbf{H}_K^{\text{HP}}) \mathbf{a}_{\mathbf{q}}. \quad (20)$$

where \mathcal{E}_0 is a constant and $\mathbf{H}_{\mathbf{q}}^{\text{HP}}$ is the exchange contribution defined in appendix A. The single-ion anisotropy Hamiltonian, which is independent of \mathbf{q} , is given by

$$\mathbf{H}_K^{\text{HP}} = \frac{\delta_{ab}}{2} \begin{bmatrix} -A_a^{\text{HP}} + C_a^{\text{HP}} & -B_a^{\text{HP}} \\ -(B_a^{\text{HP}})^\dagger & -A_a^{\text{HP}} + C_a^{\text{HP}} \end{bmatrix} \quad (21)$$

with

$$A_a^{\text{HP}} = S_a \mathbf{u}_a^T \mathbf{K}_a \mathbf{u}_a^* \left(1 - \frac{1}{S_a} (1 + 2\Phi_a) \right), \quad (22)$$

$$B_a^{\text{HP}} = S_a \mathbf{u}_a^T \mathbf{K}_a \mathbf{u}_a \left(1 - \frac{1}{4S_a} (1 + 6\Phi_a) \right), \quad (23)$$

$$C_a^{\text{HP}} = S_a \mathbf{v}_a^T \mathbf{K}_a \mathbf{v}_a \left(2 - \frac{1}{S_a} (1 + 4\Phi_a) \right), \quad (24)$$

and the magnon occupation Φ_a is defined in Eq. (A17). The terms in brackets $\frac{1}{S_a}(\dots)$ arise from the quartic Hamiltonian (17) and breaks the isotropic invariance of the K_a tensor. The magnon energies are obtained by (para)diagonalizing Eq. (20) [9, 13]. The sublattice magnetization is then calculated as

$$\langle S_a''^z \rangle = S_a - \Phi_a, \quad (25)$$

where Φ_a must be calculated self-consistently from the magnon energies. The ground state magnetization, $S_a^{(0)} = \langle S_a''^z \rangle_{T=0}$ can be obtained by evaluating Eq. (25) at $T = 0$ and satisfies $S_a^{(0)} \leq S_a$ where the equality only applies to ferromagnets. In principle, one should thus be able to calculate the critical temperature as the point where the sublattice magnetization vanishes. However, the method breaks down at elevated temperatures as the magnon energies become negative before the magnetization vanishes. The critical temperature may then be evaluated as the point where the derivative of magnetization with respect to temperature approaches $-\infty$. However, this behavior signifies a pathological feature of the HP method, which may render results at high temperatures inaccurate.

In order to analyze the dependence of the magnon gap (at $T = 0$), we consider the magnon dispersion at $T = 0$. For a Bravais lattice one obtains

$$\omega_{\mathbf{q}}^{\text{HP}} = S \sqrt{X_{\mathbf{q}}^{\text{HP}2} - |Y_{\mathbf{q}}^{\text{HP}}|^2}, \quad (26)$$

with

$$X_{\mathbf{q}}^{\text{HP}} = \frac{\mathbf{u}^T J_{\mathbf{q}}' \mathbf{u}^*}{2} - \mathbf{v}^T J_{\mathbf{q}}' \mathbf{v} + \mathbf{u}^T K \mathbf{u}^* \left(1 - \frac{1}{S}(1 + 2\Phi^0)\right) - \mathbf{v}^T K \mathbf{v} \left(2 - \frac{1}{S}(1 + 4\Phi^0)\right) \quad (27)$$

$$Y_{\mathbf{q}}^{\text{HP}} = \frac{\mathbf{u}^T J_{\mathbf{q}}' \mathbf{u}}{2} + \mathbf{u}^T K \mathbf{u} \left(1 - \frac{1}{4S}(1 + 6\Phi^0)\right). \quad (28)$$

Φ^0 is the saturation magnon number, obtained by evaluating Eq. (A17) at $T = 0$. Note that all the site indices have been dropped as we are considering a simple Bravais lattice. The magnon gap is defined as

$$\Delta = \omega_{\mathbf{q}=0} \quad (29)$$

and it is straightforward to show that the $\frac{1}{S}$ terms yield zero temperature corrections to the magnon gap. For ferromagnets Φ^0 vanishes, and the magnon gap in uniaxial systems can be expressed as

$$\Delta = K(2S - 1) \quad (30)$$

where $K = K^{zz} - K^{xx}$. We see that the magnon gap vanishes in the case of $S = 1/2$, which is the expected result. However, at finite temperatures this no longer holds and for tri-axial systems the magnon dispersion will acquire a dependence on the single-ion anisotropy at $T = 0$ for $S = 1/2$ and may even lead to instabilities (negative magnon energies). The basic reason for this failure is the truncation of $S_{ai}''^{\pm}$ in Eqs. (10)-(11), which becomes inaccurate if the anisotropy tensor couples spins that are not along the local z -axis.

B. Green's function method

The RPA Green's function approach has previously been shown to yield rather accurate predictions for critical temperatures in single- Q bulk systems [9]. Here, we extend the RPA to include single-ion anisotropy. The method is then shown to fail rather strikingly in the case of $S = 1/2$ and is expected to overestimate spinwave gaps in general. We then proceed with the Callen decoupling applied to single-ion anisotropies and show that the failure of RPA is largely remedied in this approach.

In general, the magnon energies appear as the poles of the dynamic susceptibility. Here we consider two of the (locally) transverse components, which we will just refer to as retarded Green's functions. They are defined by:

$$G_{abij}^{+-}(t) = -i\theta(t) \langle [S_{ai}''^+(t), S_{bj}''^-] \rangle \equiv \langle \langle S_{ai}''^+(t); S_{bj}''^- \rangle \rangle, \quad (31)$$

$$G_{abij}^{-}(t) = -i\theta(t) \langle [S_{ai}''^-(t), S_{bj}''^-] \rangle \equiv \langle \langle S_{ai}''^-(t); S_{bj}''^- \rangle \rangle, \quad (32)$$

where $\theta(t)$ is the Heaviside step-function. The temporal Fourier transforms are denoted by

$$G_{abij}^{\pm-}(\omega) = \int_{-\infty}^{\infty} dt e^{i(\omega+i\epsilon)t} \langle \langle S_{ai}''^{\pm}(t); S_{bj}''^- \rangle \rangle \equiv \langle \langle S_{ai}''^{\pm}; S_{bj}''^- \rangle \rangle_{\omega}, \quad (33)$$

where ϵ is an infinitesimal positive frequency that ensures convergence of the integral. Evaluating the equation of motion for the Green's functions will generate higher order (more than two operators) Green's functions that need to be approximated. In particular, the contributions from single-ion anisotropy appear in higher order Green's functions of the form

$$\langle \langle [S_{ai}''^{\pm}, \mathcal{H}_K]; S_{bj}''^- \rangle \rangle_{\omega}. \quad (34)$$

In the following we consider two decoupling approaches: the Random Phase Approximation (RPA) and the Callen decoupling (CD) scheme.

1. Random Phase Approximation

In the RPA individual spin fluctuations along the local z -axis $S_{ai}''^z$ are assumed to be small and the operator is replaced by its ensemble average $\langle S_a''^z \rangle$. This means that the three-operator Green's functions are approximated by

$$\langle \langle S_{ai}''^{\pm} S_{ai}''^z; S_{bj}''^- \rangle \rangle_{\omega} \approx \langle S_a''^z \rangle G_{abij}^{\pm-}(\omega). \quad (35)$$

Applying this, the equations of motion for the Green's functions can be written as a generalized eigenvalue equation

$$((\omega + i\epsilon)\mathbf{I} - (\mathbf{H}_{\mathbf{q}}^{\text{RPA}} + \mathbf{H}_{\mathbf{K}}^{\text{RPA}}))\mathbf{G}_{\mathbf{q}}(\omega) = \zeta, \quad (36)$$

where

$$\mathbf{G}_{\mathbf{q}}(\omega) = \sum_i [G_{ab0i}^{+-}(\omega) \ G_{ab0i}^{--}(\omega)]^T e^{i\mathbf{q}\cdot\mathbf{r}_i}, \quad (37)$$

$$\zeta = [2\langle S_a^{\prime\prime z} \rangle \delta_{ab} \ 0]^T, \quad a, b \in [1, N_a]. \quad (38)$$

Here $\mathbf{H}_{\mathbf{q}}^{\text{RPA}}$ contains the contribution from the exchange tensor, which has been derived previously [9] and is stated in appendix B. The single-ion anisotropy contribution, $\mathbf{H}_{\mathbf{K}}^{\text{RPA}}$ is given by

$$\mathbf{H}_{\mathbf{K}}^{\text{RPA}} = \delta_{ab} \begin{bmatrix} -\mathbf{A}_a^{\text{RPA}} + \mathbf{C}_a^{\text{RPA}} & -\mathbf{B}_a^{\text{RPA}} \\ (\mathbf{B}_a^{\text{RPA}})^\dagger & \mathbf{A}_a^{\text{RPA}} - \mathbf{C}_a^{\text{RPA}} \end{bmatrix} \quad (39)$$

with

$$\mathbf{A}_a^{\text{RPA}} = \langle S_a^{\prime\prime z} \rangle \mathbf{u}_a^T \mathbf{K}_a \mathbf{u}_a^*, \quad (40)$$

$$\mathbf{B}_a^{\text{RPA}} = \langle S_a^{\prime\prime z} \rangle \mathbf{u}_a^T \mathbf{K}_a \mathbf{v}_a, \quad (41)$$

$$\mathbf{C}_a^{\text{RPA}} = 2\langle S_a^{\prime\prime z} \rangle \mathbf{v}_a^T \mathbf{K}_a \mathbf{v}_a. \quad (42)$$

Unlike HP, the isotropic invariance of the tensor \mathbf{K}_a is preserved in RPA. This is easily seen by noting that $\mathbf{u}_a^T \mathbf{u}_a^* = 2$, $\mathbf{u}_a^T \mathbf{v}_a = 0$, and $\mathbf{v}_a^T \mathbf{v}_a = 1$.

Similar to HP, we can calculate the magnon energies at $T = 0$ for a Bravais lattice using RPA. The result is

$$\omega_{\mathbf{q}}^{\text{RPA}} = S^{(0)} \sqrt{X_{\mathbf{q}}^{\text{RPA}2} - |Y_{\mathbf{q}}^{\text{RPA}}|^2}, \quad (43)$$

where $S^{(0)}$ is the saturation magnetization calculated as in Eq. (58) and

$$X_{\mathbf{q}}^{\text{RPA}} = \frac{\mathbf{u}^T (\mathbf{J}'_{\mathbf{q}} + 2\mathbf{K}) \mathbf{u}^*}{2} - \mathbf{v}^T (\mathbf{J}'_{\mathbf{q}} + 2\mathbf{K}) \mathbf{v}, \quad (44)$$

$$Y_{\mathbf{q}}^{\text{RPA}} = \frac{\mathbf{u}^T (\mathbf{J}'_{\mathbf{q}} + 2\mathbf{K}) \mathbf{u}}{2}. \quad (45)$$

It can be observed that RPA predicts a finite gap for $S = 1/2$ and fails to capture the irrelevance of single-ion anisotropy in this case. This is a serious flaw of the method, which we address by turning to the CD scheme for the single-ion anisotropy.

2. Callen decoupling

As RPA assumes the fluctuations in $S_{ai}^{\prime\prime z}$ to be small, the large fluctuations that would become relevant at higher temperatures are disregarded *a priori*. The CD attempts to generalize the RPA mean-field approach in such a way that fluctuations in $S_{ai}^{\prime\prime z}$ become important at high temperatures [14, 17]. However, comparing results with quantum Monte Carlo simulations for $S = 1/2$ ferromagnets reveals that the method actually yields worse results than RPA [16]. For higher spins it is expected to become more accurate and for itinerant systems (treated in the classical limit) the CD was found to be more accurate than RPA [15]. Moreover, it has been shown that

the CD predicts much better results than RPA when it is solely applied to single-ion anisotropy in ferromagnets [15, 16]. One reason for this is that it predicts the correct lack of order in $S = 1/2$ and is not subject to the overestimation of spinwave gaps inherent to RPA. As the failure of RPA for single-ion anisotropy is not limited to ferromagnets, we derive a single- Q generalization of the CD for single-ion anisotropy. Combined with the RPA Hamiltonian for the exchange thus yields the hybrid RPA+CD approach.

The central idea in CD is parameterizing the three different representations of the $S_{ai}^{\prime\prime z}$ operator:

$$S_{ai}^{\prime\prime z} = S_a(S_a + 1) - S_{ai}^{\prime\prime -} S_{ai}^{\prime\prime +} - S_{ai}^{\prime\prime z2}, \quad (46)$$

$$S_{ai}^{\prime\prime z} = -S_a(S_a + 1) + S_{ai}^{\prime\prime +} S_{ai}^{\prime\prime -} + S_{ai}^{\prime\prime z2}, \quad (47)$$

$$S_{ai}^{\prime\prime z} = \frac{S_{ai}^{\prime\prime +} S_{ai}^{\prime\prime -} - S_{ai}^{\prime\prime -} S_{ai}^{\prime\prime +}}{2}. \quad (48)$$

Introducing the parameter $\alpha \in \{-1, 0, 1\}$ these equations can be combined into a single one:

$$S_{ai}^{\prime\prime z} = \alpha(S_a(S_a + 1) - S_{ai}^{\prime\prime z2}) + \frac{1}{2}(1 - \alpha)S_{ai}^{\prime\prime +} S_{ai}^{\prime\prime -} - \frac{1}{2}(1 + \alpha)S_{ai}^{\prime\prime -} S_{ai}^{\prime\prime +}. \quad (49)$$

The point is now that the decoupling will depend on the choice of α and Callen argued that α should be chosen differently for the low and high temperature regimes. Applying the parameterized representation of $S_{ai}^{\prime\prime z}$, the higher-order Green's functions can be symmetrically decoupled as

$$\langle \langle S_{ai}^{\prime\prime \pm} S_{ai}^{\prime\prime z}; S_{bj}^{\prime\prime -} \rangle \rangle_{\omega} \approx (\langle S_a^{\prime\prime z} \rangle - \alpha \langle S_{ai}^{\prime\prime \pm} S_{ai}^{\prime\prime \mp} \rangle) G_{abij}^{\pm-}(\omega), \quad (50)$$

and the parameter α can be chosen as $\frac{\langle S_a^{\prime\prime z} \rangle}{2S_a^2}$ which will interpolate between 1 and 0 for $T = 0$ and $T = T_C$ respectively. Applying this to Eq. (50), the CD single-ion anisotropy Hamiltonian is obtained as

$$[\mathbf{H}_{\mathbf{K}}^{\text{CD}}]_{\alpha\beta} = [\mathbf{H}_{\mathbf{K}}^{\text{RPA}}]_{\alpha\beta} \left(1 - \frac{\langle S_a^{\prime\prime z} \rangle}{2S_a^2} (1 + 2\Phi_a) \right) \delta_{\alpha\beta}, \quad (51)$$

where $\alpha, \beta \in [1, 2N_a]$, $\mathbf{H}_{\mathbf{K}}^{\text{RPA}}$ is defined in Eq. (39) and Φ_a is the magnon occupation number defined in Eq. (54). The magnon energies within the RPA+CD method can be obtained by solving the eigenvalue equation (36) with the single-ion anisotropy contribution $\mathbf{H}_{\mathbf{K}}^{\text{RPA}}$ replaced by $\mathbf{H}_{\mathbf{K}}^{\text{CD}}$.

Analyzing the behavior of single-ion anisotropy in RPA+CD, we find

$$\mathbf{H}_{\mathbf{K}}^{\text{CD}}(T = 0) \propto \left(1 - \frac{(S_a - \Phi_a^0)(1 + 2\Phi_a^0)}{2S_a^2} \right) \quad (52)$$

where Φ^0 is defined in Eq. (59). It is observed that for $S = 1/2$, this contribution is close to being independent of K_a , as the quantity in bracket is close to (exactly

for ferromagnets) zero. Importantly, it is RPA+CD that yields the closest agreement to the true behavior (irrelevance) of single-ion anisotropy in $S = 1/2$ systems when comparing the three methods considered here. It is also easy to see that the isotropic invariance of RPA is preserved by CD.

3. Magnetization and Critical temperature

In the Green's function approach, the (sublattice) magnetization is given by [9, 14, 15]

$$\langle S_a''z \rangle = \frac{(S_a - \Phi_a)(1 + \Phi_a)^{2S_a+1} + (S_a + 1 + \Phi_a)\Phi_a^{2S_a+1}}{(1 + \Phi_a)^{2S_a+1} - \Phi_a^{2S_a+1}}, \quad (53)$$

where Φ_a is the site-resolved magnon occupation calculated from the fluctuation-dissipation theorem as

$$\Phi_a = \frac{1}{N} \sum_{\eta, \mathbf{q}} U_{a\eta\mathbf{q}} n_B(\omega_{\eta, \mathbf{q}}) U_{\eta a \mathbf{q}}^{-1}, \quad (54)$$

where and $U_{a\eta\mathbf{q}}$ is the matrix that diagonalizes

$$\mathbf{H}_{\mathbf{q}}^{\text{RPA}} + \mathbf{H}_{\mathbf{K}}^{\text{RPA/CD}} \quad (55)$$

and $\omega_{\eta, \mathbf{q}}$ are the eigenvalues. We note that in Eqs. (53)-(54), $a \in \{1, \dots, N_a\}$, but the sum in (54) runs over all ($2N_a$) eigenfrequencies for a given \mathbf{q} . The Bose factor $n_B(\omega_{\eta, \mathbf{q}})$ is given by

$$n_B(\omega_{\eta, \mathbf{q}}) = \frac{1}{e^{\omega_{\eta\mathbf{q}}/k_B T} - 1}, \quad (56)$$

and is thus evaluated at positive as well as negative eigenfrequencies although only the positive eigenvalues are interpreted as magnon energies. For each temperature, the magnetization must be calculated self-consistently since the Hamiltonian depends on the Bose factors and the magnon energies are thus renormalized (softened) at finite temperatures.

In the limit of small Φ , Eq. (53) can be expanded as

$$\langle S_a''z \rangle = S_a - \Phi_a + \mathcal{O}(\Phi^{2S_a+1}). \quad (57)$$

At zero temperature, this reduces to the saturation magnetization, $S_a^{(0)}$, given by

$$S_a^{(0)} = \langle S_a''z \rangle_{T=0} = S_a - \Phi_a^0 \quad (58)$$

with

$$\Phi_a^0 = -\frac{1}{N} \sum_{\mathbf{q}} \sum_{n=1}^{N_a} U_{a n \mathbf{q}} U_{n a \mathbf{q}}^{-1}, \quad (59)$$

where we used

$$n_B^{T=0}(\omega_{\eta\mathbf{q}}) = \begin{cases} -1, & \eta \in [1, N_a] \\ 0, & \eta \in (N_a, 2N_a] \end{cases}. \quad (60)$$

Note that the above equation assumes that all the eigenvectors are sorted according to the ascending eigenvalues. Except for ferromagnets, the saturation magnon number will be non-vanishing and $S_a^{(0)} < S_a$. In contrast to the HP approach, the magnetization calculated from Eq. (53) will yield a function of temperature, which smoothly approaches zero as we reach the critical temperature. For systems with equivalent site magnetization, $\langle S_a''z \rangle = \langle S''z \rangle \forall a$, we can obtain an analytical expression for the RPA critical temperature by expanding Eq. (53) in the limit of $\langle S''z \rangle \rightarrow 0$:

$$k_B T_C^{\text{RPA}} = \frac{S(S+1)}{3} \left(\frac{\langle S''z \rangle}{N} \sum_{\eta\mathbf{q}} \frac{U_{0\eta\mathbf{q}} U_{\eta 0 \mathbf{q}}^{-1}}{\omega_{\eta, \mathbf{q}}} \right)^{-1}. \quad (61)$$

Since $\omega_{\eta, \mathbf{q}}$ is proportional to $\langle S''z \rangle$, the expression effectively no longer depends on it. This is a generalization of the critical temperature of a Bravais lattice derived in our previous work [9] to non-Bravais lattices with equivalent spin sites. For the RPA+CD approach, the critical temperature must be obtained from a numerical (self-consistent) calculation of the magnetization curve.

C. Critical temperatures in the limit of small anisotropies

The Mermin-Wagner theorem has established that magnetic anisotropy plays a pivotal role in the magnetic order in 2D materials. Here we study the behavior of the critical temperature in the limit of small magnon gaps, corresponding to the regime of weak magnetic anisotropy. We analyze the cases of simple ferromagnetic and anti-ferromagnetic order with uniaxial anisotropy using RPA.

For ferromagnetic order, the magnon dispersion is quadratic in the vicinity of $\mathbf{q} = 0$ and the magnon gap (Δ_{FM}) is linear with respect to the anisotropy strength. Assuming an isotropic lattice, it can be expressed as

$$\omega_{\mathbf{q}}^{\text{FM}} = \langle S''z \rangle (bq^2 + \Delta_{\text{FM}}) \quad (62)$$

For $\omega_{\mathbf{q}} \ll k_B T$, the Bose factor in Eq. (56) can be expanded as

$$n_B(\omega_{\eta, \mathbf{q}}) \approx \begin{cases} -\frac{k_B T}{\omega_{\mathbf{q}}} & \eta = 1 \\ +\frac{k_B T}{\omega_{\mathbf{q}}} & \eta = 2 \end{cases}. \quad (63)$$

If the magnon gap becomes small, the largest contribution of the magnon number Eq. (54) will originate from the vicinity of $\mathbf{q} = 0$. This contribution can be separated from the rest such that

$$\Phi = \frac{2}{q_c^2 \langle S''z \rangle} \int_0^{q_c} k_B T \frac{q dq}{bq^2 + \Delta_{\text{FM}}} + \sum_{|\mathbf{q}| > q_c} \dots, \quad (64)$$

where q_c is some small cutoff and the second term will become irrelevant if the anisotropy is sufficiently small.

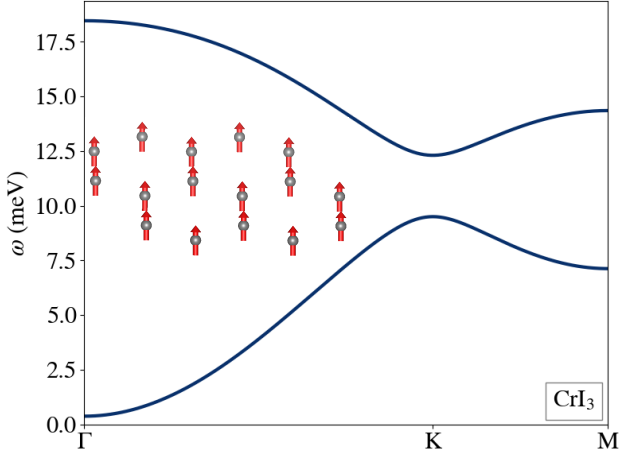


Figure 1. The magnon dispersion of monolayer CrI_3 calculated using bulk INS parameters from Ref. [19]. A DM interaction of 0.09 meV in the out-of-plane direction opens a topological gap at the high symmetry point K. The inset shows the magnetic lattice of CrI_3 .

The magnetization in Eq. (53) can be expanded in the limit of large Φ ($\langle S''^z \rangle \rightarrow 0$) as

$$\langle S''^z \rangle \approx \frac{S(S+1)}{3\Phi}, \quad (65)$$

$$= \frac{S(S+1)}{3} \left(\frac{2}{q_c^2 \langle S''^z \rangle} \int_0^{q_c} k_B T \frac{q dq}{bq^2 + \Delta_{\text{FM}}} \right)^{-1}, \quad (66)$$

which becomes exact as $T \rightarrow T_C$ and one obtains

$$k_B T_C^{\text{RPA}} \propto \left[\ln \left(\frac{bq_c^2 + \Delta_{\text{FM}}}{\Delta_{\text{FM}}} \right) \right]^{-1}. \quad (67)$$

The Curie temperature thus acquires a logarithmic dependence on the gap in the limit of small gaps.

For anti-ferromagnetic order, we consider the simple case of a quadratic lattice. In the vicinity of $\mathbf{q} = 0$, the magnon dispersion becomes hyperbolic:

$$\omega_{\mathbf{q}}^{\text{AFM}} = \langle S''^z \rangle \sqrt{cq^2 + \Delta_{\text{AFM}}^2}. \quad (68)$$

Performing the same steps as above in the limit of small anisotropy then yields

$$k_B T_N^{\text{RPA}} \propto \left[\ln \left(\frac{cq_c^2 + \Delta_{\text{AFM}}^2}{\Delta_{\text{AFM}}^2} \right) \right]^{-1}. \quad (69)$$

Note that there is an additional term proportional to $(cq^2 + \Delta_{\text{AFM}}^2)^{-1/2}$ originating from the eigenvectors when evaluating Eq. (54) for anti-ferromagnets.

D. Dipole interactions

In addition to exchange and single-ion anisotropy, long range dipole-dipole interactions can also play an important role in two-dimensional magnetic materials. These

interactions arise from the magnetic dipole moments of the ions and decay as $1/r^3$, leading to a long range contribution to the spin Hamiltonian. In the extended Heisenberg model, the dipolar term can be written as

$$\mathcal{H}_{\text{dip}} = \frac{\mu_0}{8\pi} \sum_{abij} \left(\frac{\mathbf{m}_{ai} \cdot \mathbf{m}_{bj}}{|\mathbf{r}_{abij}|^3} - \frac{3(\mathbf{m}_{ai} \cdot \mathbf{r}_{abij})(\mathbf{m}_{bj} \cdot \mathbf{r}_{abij})}{|\mathbf{r}_{abij}|^5} \right), \quad (70)$$

where μ_0 is the vacuum permeability. The magnetic moment is related to the spin by $\mathbf{m}_{ai} = -g\mu_B \mathbf{S}_{ai}$, where g is the spin g -factor and μ_B is the Bohr magneton. This term can introduce long range anisotropic couplings and may play a role in stabilizing magnetic order in 2D in systems when spin-orbit coupling is weak. If the magnitude of the dipole-dipole interaction is comparable to the exchange energies, it may also modify the magnon spectra. In the methodology introduced above, the dipole interactions can be incorporated as a simple addition to the exchange tensor:

$$\mathbf{J}_{ab\mathbf{q}} \rightarrow \mathbf{J}_{ab\mathbf{q}} - D_{ab\mathbf{q}}, \quad (71)$$

$$[D_{ab\mathbf{q}}]^{\mu\nu} = \frac{D}{N} \sum_{ij} \left(\frac{\delta_{\mu\nu}}{|\mathbf{r}_{abij}|^3} - \frac{3[\mathbf{r}_{abij}]^\mu [\mathbf{r}_{abij}]^\nu}{|\mathbf{r}_{abij}|^5} \right) e^{i\mathbf{q} \cdot \mathbf{r}_{ij}}, \quad (72)$$

$$D = \frac{\mu_0}{4\pi} g^2 \mu_B^2. \quad (73)$$

Since the dipolar interaction is inherently long ranged, the dipole tensor in Eq. (72) must be evaluated to sufficiently large distances until the summation converges. Unlike the single-ion anisotropy, the dipolar anisotropy is dispersive (q -dependent) and therefore manifests itself differently in the magnon spectrum.

III. RESULTS

We have introduced three different approaches to study the thermal renormalization of magnon energies and critical temperatures for single- Q states including single-ion anisotropy. We now benchmark the methods on different 2D magnetic materials using exchange constants obtained from inelastic neutron scattering experiments on their bulk parent compounds. In particular, we take CrI_3 , MPS_3 ($M=\text{Ni}, \text{Mn}, \text{Fe}$) and CrSBr , and show that the Heisenberg parameters reproduce the experimental magnon dispersions at zero temperature. We then calculate the critical temperature using HP, RPA, RPA+CD and classical Monte Carlo simulations and compare the results with experimental values.

A. CrI_3

CrI_3 was the first material shown to exhibit long-range ferromagnetic order in the monolayer limit [1]. The Cr atoms form a honeycomb lattice and exhibits strong easy-axis uniaxial anisotropy. In fact, the three-fold rotational

symmetry associated with each magnetic site renders the single-ion anisotropy tensor diagonal with $K_a^{xx} = K_a^{yy}$, and we are free to set these in-plane components to zero. The single-ion anisotropy is thus completely characterized by K_a^{zz} . Since its discovery, there has been considerable interest in this material - theoretical as well as experimental [20, 21]. The Cr atoms are in the 3+ oxidation state and are well represented by $S = 3/2$ sites in a Heisenberg model. Since CrI_3 is ferromagnetic, there is no reduction in the saturation magnetization, which is simply given by $S_a^{(0)} = 3/2$ as well. The Heisenberg exchange and anisotropy parameters extracted from inelastic neutron scattering (INS) experiments of bulk CrI_3 [19] are listed in Tab. I. As we are interested in the monolayer limit, the interlayer exchange is not included in our calculations, but we assume that the Heisenberg parameters for a single monolayer are well approximated by those of the bulk material. The Dzyaloshinskii–Moriya (DM) interaction in CrI_3 is absent in the nearest neighbor bond (due to an inversion center), but appears between next nearest neighbors. It is reported to be relatively weak compared to the exchange constants, with a magnitude of 0.09 meV [19], but gives rise to a sizable gap between the acoustic and optical magnon branches. At the level of linear spin-wave theory it is only the out-plane component that opens such a gap and the remaining components are typically disregarded although they are not forbidden by symmetry in CrI_3 . The gap between the magnon branches is topological (finite Chern number) and has been discussed extensively in the literature [19, 22, 23]. In the present tensor notation, these out-of-plane DM component enter as intra-sublattice components $J_{aaij}^{xy}/2 = -J_{aaij}^{yx}/2$, where i and j denote neighboring cells. Since single-ion anisotropy contributes differently to the magnon dispersion for HP and RPA treatments, the reported experimental values depend on which method the dispersion was fitted to. We have thus recalculated the uniaxial single-ion anisotropy constant, K_a^{zz} , directly from the experimentally observed spin-wave gap, obtaining a value of 0.184 meV for RPA+CD (and HP) and 0.123 meV for RPA. This recalculation ensures a consistent treatment of anisotropy within our formalism and ensures that the calculated spinwave dispersion agrees with the experimental one regardless of the methodology. We note that a similar analysis was performed in our previous work on CrI_3 [15], but in that case we employed exchange constants extracted from optical magnon energies and the spin-wave gap of bilayer CrI_3 reported in Ref. [24]. In contrast, here we base our analysis on the full magnon spectrum of bulk CrI_3 measured via INS experiments, providing a more comprehensive and accurate parameter set.

The magnon dispersion along the high-symmetry path Γ –K–M (with INS parameters from Ref. [19]) is shown in Fig. 1 and the corresponding critical temperatures obtained using MC, HP, RPA, and RPA+CD methods are summarized in Tab. III. It is observed that the RPA+CD approach yields the closest agreement to the experimen-

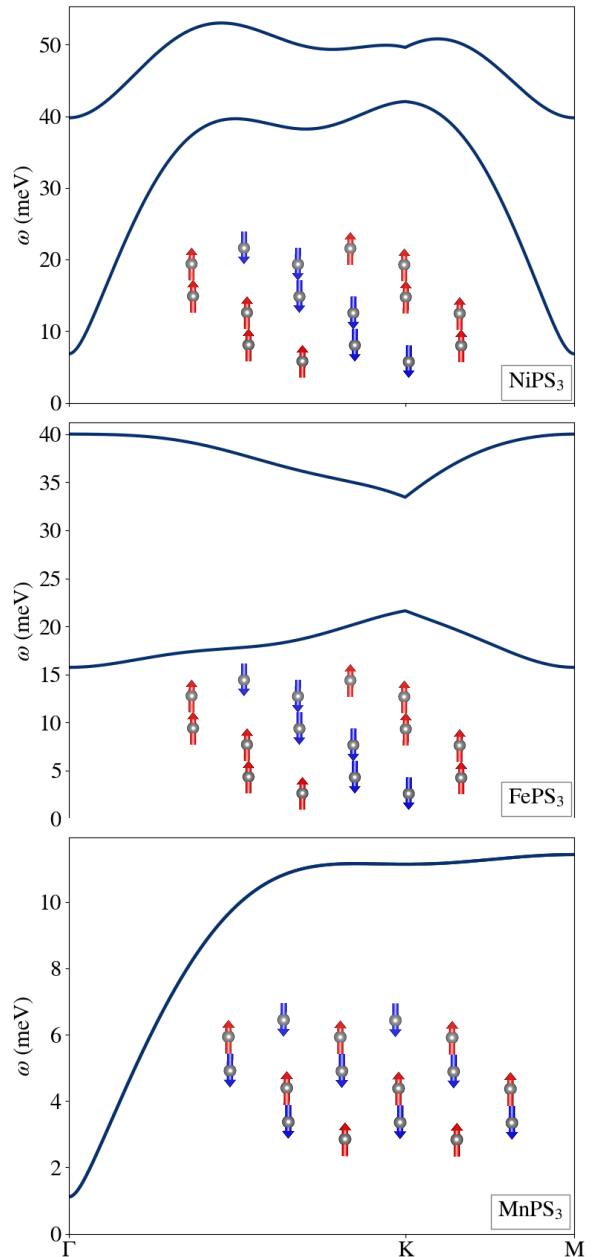


Figure 2. The magnon dispersion relations of monolayer MPS_3 ($M=\text{Ni, Fe, Mn}$) anti-ferromagnets with Heisenberg parameters taken from INS [25]. The inset shows the magnetic lattices with the corresponding ground state magnetic order.

tal critical temperature, which is consistent with previous work [15] based on parameters from bilayer CrI_3 .

B. MPS_3

The MPS_3 ($M=\text{Ni, Mn, Fe}$) compounds comprise a family of layered transition-metal thiophosphates that crystallize with a honeycomb arrangement of transition-

	J_1	J_2	J_3	K^{zz}
CrI ₃	2.11	0.11	-0.10	0.123 (0.184)
NiPS ₃	3.8	-0.2	-13.80	0.3 (0.6)
FePS ₃	2.92	-0.08	-1.92	2.66 (3.55)
MnPS ₃	-1.54	-0.14	-0.36	0.0086 (0.0108)

Table I. In-plane exchange and anisotropy constants of bulk CrI₃ [19] and MPS₃ (M=Ni, Fe, Mn) [25] taken from INS experiments ($K^{xx} = K^{yy} = 0$). All numbers are meV. The anisotropy constants are calculated from the spin-wave dispersion by fitting to either RPA or HP/RPA+CD (shown in brackets).

metal ions within each layer. Here, we consider NiPS₃, FePS₃ and MnPS₃, which gives rise to layered anti-ferromagnetic ordering with uniaxial anisotropy [26–30]. NiPS₃ and FePS₃ exhibit a zig-zag magnetic ordering in the ab -plane with an in-plane ordering vector $\mathbf{Q} = [1/2, 0]$, where spins in the unit cell are parallel with $S = 1$ and $S = 2$ respectively. MnPS₃, on the other hand exhibits Néel order, where all the nearest neighbors are anti-parallel and is represented by a $\mathbf{Q} = [0, 0]$ in-plane ordering vector with anti-parallel spins in the primitive unit cell and $S = 5/2$. The exchange and anisotropy parameters of these compounds have been studied extensively in the literature using both experimental [25, 28–30] and first principles approaches [31, 32]. Similar to the case of CrI₃, symmetry dictates that the single-ion anisotropy is completely characterized by $K_a^{zz} = K^{zz}$. For the purpose of benchmarking our methods, we use the Heisenberg parameters obtained from the bulk INS data reported in Ref. [25], and the values are tabulated in Tab. I. The calculated magnon dispersions for the three compounds are shown in fig. 2, along with the magnetic structure. Since these materials are anti-ferromagnets, the exchange constants (J_n) from the experimental fit performed with linear spin wave theory differ from RPA/RPA+CD by a factor of $S_a/\langle S_a^{zz} \rangle$. To avoid confusion, we have retained the original unscaled exchange constants and assumed $S_a^{(0)} = S_a$ in our calculations.

The Néel temperatures calculated using different approaches using INS data are tabulated in Tab. III, and we observe that RPA+CD shows the closest agreement with experiments for NiPS₃. Since MnPS₃ has very weak anisotropy, the CD correction does not make a significant difference compared to RPA, and the latter shows slightly closer agreement with the experimental value. The parameters reported in Ref. [25] describe the anisotropy energy of MnPS₃ exclusively through the single-ion contribution, while the dipolar contribution, reported to have a comparable magnitude ($\Delta E_{\text{dip}}^{xz} \approx 54 \mu\text{eV}/\text{site}$) [32], was not included in the analysis. Fitting the Heisenberg parameters of MnPS₃ to a model that includes dipolar interactions, would likely comprise a more accurate approach, but we have not attempted that here. In the case of FePS₃, the RPA/RPA+CD deviates significantly from the experimental value although RPA+CD yields a

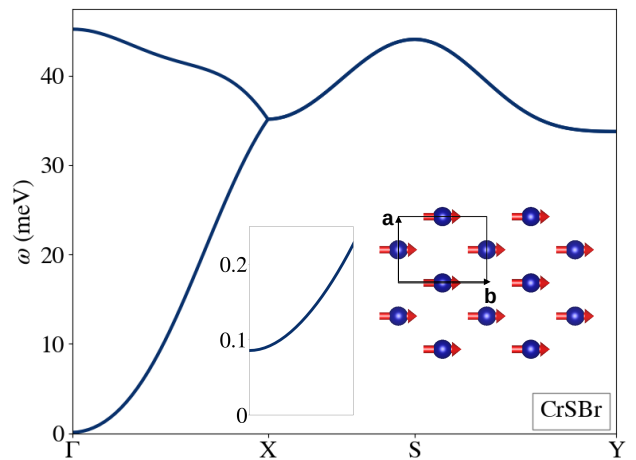


Figure 3. The magnon dispersion of CrSBr calculated from the experimental parameters listed in tab. II. The inset shows the real space arrangement of magnetic atoms.

somewhat better agreement than RPA. The HP method, while giving the closest agreement with experiment, generally exhibits a pathological behavior with discontinuous magnetization near the Néel temperature [9, 15], and therefore cannot be regarded as a reliable result in our opinion. It has previously been shown that both RPA, RPA+CD and HP severely overestimate critical temperatures when the anisotropy becomes large and all methods are thus expected to be inaccurate for FePS₃, which have $K^{zz}/J_1 \sim 1$. Moreover, the magnetic anisotropy in the INS data was solely fitted with the quadratic single-ion anisotropy term in the Hamiltonian. However, first principle calculations reveal that FePS₃ exhibits a fully unquenched orbital moment aligned with the out-of-plane direction [32, 33] and the anisotropy is probably better described by an $\mathbf{L} \cdot \mathbf{S}$ term in the Hamiltonian (with fixed \mathbf{L}), which may give rise to a different behavior compared to single-ion anisotropy.

C. CrSBr

CrSBr is a layered van der Waals bonded anti-ferromagnetic semiconductor, in which the individual ferromagnetic layers are coupled anti-ferromagnetically [34–36]. The ferromagnetic monolayer has been exfoliated from bulk and exhibits a remarkably high Curie temperature of 146 K [37–40]. The Cr³⁺ magnetic ions form a rectangular lattice with a ground state spin of $S = 3/2$. In addition, it is notable for exhibiting triaxial magnetic anisotropy, with distinct easy, intermediate, and hard axes [41, 42].

The Heisenberg parameters of CrSBr used in this work are compiled from two experimental references. The isotropic exchange interactions of bulk CrSBr are taken from Ref. [43] where the anisotropy was reported too weak to be measured. Since anisotropy is a crucial pa-

CrSBr	
J_1	1.9
J_2	3.38
J_3	1.67
J_4	0.09
J_5	0.09
J_7	-0.37
J_8	0.29
K_a^{xx}	0.044/0.066/0.038
K_a^{yy}	0.058/0.087/0.073
K_a^{zz}	0.0/0.0/0.0

Table II. In-plane exchange constants (in meV) of bulk CrSBr taken from Ref. [43]. J_6 is omitted as it corresponds to interlayer exchange in the layered compound. The anisotropy parameters (in meV) are taken from spectroscopic measurements [41] and are converted (using isotropic invariance) such that the hard axis anisotropy component (K_a^{zz}) is zero. The values are listed for RPA/RPA+CD/HP, which are obtained by fitting the predicted dispersion relations to the experimental one.

parameter for magnetic order, we use the values reported in Ref. [41] where the hard and intermediate anisotropy parameters are obtained from anti-ferromagnetic resonance experiments. In CrSBr, the hard axis is along the c -axis, the intermediate is the a -axis and the easy axis is the b -axis. The point group of the monolayer is mmm and the mirror symmetries enforce all off-diagonal elements of the single-ion anisotropy tensors to vanish. We will again use the isotropic invariance of Eq. (2) to set the hard axis components K_a^{zz} to zero and we convert the values stated in Ref. [41] to our conventions with a full characterization given by the components K_a^{xx} and K_a^{yy} .

The calculated magnon dispersion of CrSBr is shown in fig. III B and the exchange and anisotropy parameters used in the calculations are tabulated in tab. II. Unlike the uniaxial case, the HP and RPA+CD magnon gap differ at zero temperature due to the different in-plane components of magnetic anisotropy. Hence, the components of K_a have to be properly refitted for HP and RPA+CD to ensure that the same magnon dispersion is obtained for all three methods. The magnon gap induced by triaxial anisotropy is two orders of magnitude smaller than the magnon band width, yet it plays a crucial role in stabilizing the magnetic order in CrSBr. The Curie temperatures calculated using different approaches are summarized in tab. III, and again RPA+CD shows the best agreement with the experimental value.

IV. CONCLUSION

We have extended the theoretical approaches for calculating critical temperatures of single- Q 2D magnetic materials - emphasizing the role of single-ion anisotropy. We studied the HP approach, and observed that normal ordering of the fourth order bosonic operators yield second-order corrections to the zero temperature magnon

	MC	HP	RPA	RPA+CD	Expt
CrI ₃	15	20	52	47	45
NiPS ₃	85	100	167	157	155*
MnPS ₃	55	44	67	64	78*
FePS ₃	90	118	266	215	120*
CrSBr	56	95	151	150	146

Table III. Calculated critical temperatures (in K) of the materials considered in this work. The experimental values marked with a star are critical temperatures in the bulk compounds, while the remaining ones (including all calculations) are for monolayers.

energies. These corrections capture the correct behavior of uniaxial single-ion anisotropy for ferromagnets, but not for anti-ferromagnets or for general systems with triaxial anisotropy. The corrections also fail to conserve the isotropic invariance of single-ion anisotropy terms because of an incomplete bosonic expansion of the transverse spin components. We then studied the RPA decoupling scheme applied to the single ion anisotropy terms and it was shown that RPA conserves the isotropic invariance but fails to reproduce the correct spin-wave gap - in particular the irrelevance of single-ion anisotropy for $S = 1/2$. Finally, we extended Callen's decoupling scheme to include the single-ion anisotropy tensor of any single- Q system. In contrast to RPA, CD captures the correct spin-wave gap and irrelevance of single-ion anisotropy for $S = 1/2$ ferromagnets. Moreover, in contrast to HP it conserves the isotropic invariance and its accuracy is not restricted to uniaxial cases. On the basis of fundamental theoretical arguments, we expect CD to provide the best description of single-ion anisotropy. For magnon dispersion relations, we thus adopt a hybrid RPA+CD approach, using Callen's decoupling for the single-ion anisotropy and RPA for the remaining interactions. This combination has also been shown to yield the best agreement with quantum Monte Carlo results for ferromagnets [16].

We applied the three methods to a set of two-dimensional materials with exchange parameters taken from experiments and compared the calculated critical temperatures to experimental values. In comparison with experimental critical temperatures, we found that RPA+CD gives the best performance, except for MnPS₃ and FePS₃. For MnPS₃, which is nearly isotropic with only a weak uniaxial anisotropy, the application of the CD correction yields a negligible deviation from the RPA results. In addition, incorporating the dipolar contribution into the fit of the magnon anisotropy from INS data would likely improve the precision of the results. In the case of FePS₃, the the Fe atoms carry a large orbital moment, which is pinned to the lattice and strongly coupled to the spin. This indicates that a simple single-ion anisotropy tensor is likely insufficient to fully describe the magnetic anisotropy. In any case, the RPA+CD approach was found perform better than RPA, while HP yields excellent agreement with the experimental value.

However, we believe that this is a fortuitous result originating in error cancelation within that method.

In summary, we presented a comprehensive analysis of the role of single-ion anisotropy in calculating thermally excited magnon energies and critical temperatures in two dimensional magnets. Among the methods considered, the RPA+CD approach showed the best agreement with experiments, establishing it as the best method for predicting critical temperatures in low-dimensional systems. This approach comprises a simple and versatile method that is easily applicable and is expected to significantly improve the accuracy of either classical Monte Carlo simulations or linear spin wave theory, which seems to be the most common approaches in the literature. The framework can also be used to analyze the influence of complex spin interactions, such as anisotropic exchange, Dzyaloshinskii-Moriya interaction, dipole-dipole interactions and higher order terms like biquadratic exchange. As such, we believe that the RPA+CD approach provides the most reliable route for understanding and predicting thermal properties of 2D materials.

Appendix A: Exchange contribution to the HP Hamiltonian

The exchange contribution to the constant in Eq. (20) is

$$\mathcal{E}_0 = -\frac{1}{2} \sum_{abij} \mathbf{v}_a^T J'_{abij} \mathbf{v}_b (S_a S_b + \frac{S_a + S_b}{2}), \quad (\text{A1})$$

and the exchange contribution to the quadratic Hamiltonian is

$$H_{\mathbf{q}}^{\text{HP}} = H_{\mathbf{q}}^0 + H_{\mathbf{q}}^1, \quad (\text{A2})$$

$$H_{\mathbf{q}}^0 = -\frac{1}{2} \begin{bmatrix} A_{ab\mathbf{q}}^0 - C_{ab}^0 & B_{ab\mathbf{q}}^0 \\ B_{ab\mathbf{q}}^{0\dagger} & A_{ab-\mathbf{q}}^{0*} - C_{ab}^0 \end{bmatrix}, \quad (\text{A3})$$

$$H_{\mathbf{q}}^1 = \frac{1}{2} \begin{bmatrix} A_{ab\mathbf{q}}^1 - C_{ab\mathbf{q}}^1 & B_{ab\mathbf{q}}^1 \\ B_{ab\mathbf{q}}^{1\dagger} & A_{ab-\mathbf{q}}^{1*} - C_{ab\mathbf{q}}^{1*} \end{bmatrix}, \quad (\text{A4})$$

with

$$A_{ab\mathbf{q}}^0 = \frac{\sqrt{S_a S_b}}{2} \mathbf{u}_a^T J'_{ab\mathbf{q}} \mathbf{u}_b^*, \quad (\text{A5})$$

$$B_{ab\mathbf{q}}^0 = \frac{\sqrt{S_a S_b}}{2} \mathbf{u}_a^T J'_{ab\mathbf{q}} \mathbf{u}_b, \quad (\text{A6})$$

$$C_{ab}^0 = \delta_{ab} \sum_c S_c \mathbf{v}_a^T J'_{ac0} \mathbf{v}_c, \quad (\text{A7})$$

and

$$A_{ab\mathbf{q}}^1 = \frac{1}{N} \sum_{\mathbf{q}'} \left(\mathbf{u}_a^T J'_{ab\mathbf{q}} \mathbf{u}_b^* \frac{n_{aa\mathbf{q}'} + n_{bb\mathbf{q}'}}{4} + \delta_{ab} \sum_c \frac{\mathbf{u}_c^T J'_{ca\mathbf{q}'} \mathbf{u}_a^* n_{ca\mathbf{q}'} + \mathbf{u}_a^T J'_{ac\mathbf{q}'} \mathbf{u}_c^* n_{ac\mathbf{q}'}}{4} \right), \quad (\text{A8})$$

$$B_{ab\mathbf{q}}^1 = \frac{1}{N} \sum_{\mathbf{q}'} \left(\mathbf{u}_a^T J'_{ab\mathbf{q}} \mathbf{u}_b \frac{n_{aa\mathbf{q}'} + n_{bb\mathbf{q}'}}{4} + \delta_{ab} \sum_c \frac{\mathbf{u}_a^T J'_{ac\mathbf{q}'} \mathbf{u}_c n_{ac\mathbf{q}'} + \mathbf{u}_c^T J'_{ac\mathbf{q}'} \mathbf{u}_a n_{ac\mathbf{q}'}}{8} \right), \quad (\text{A9})$$

$$C_{ab\mathbf{q}}^1 = \frac{1}{N} \sum_{\mathbf{q}'} \left(\mathbf{v}_a^T J'_{ab\mathbf{q}-\mathbf{q}'} \mathbf{v}_b n_{ba\mathbf{q}'} + \delta_{ab} \sum_c n_{cc\mathbf{q}'} \mathbf{v}_a^T J'_{ac0} \mathbf{v}_c \right). \quad (\text{A10})$$

Note that the expressions here are slightly different from the ones presented in Ref. [9] because we have separated the single-ion anisotropy tensor from $J_{ab\mathbf{q}}$. Here the q -space exchange interactions are defined as

$$J'_{ab\mathbf{q}} = \sum_i J_{ab0i} e^{i\mathbf{q} \cdot \mathbf{r}_i}, \quad (\text{A11})$$

$$J'_{abij} = \mathbf{R}_i^T J_{abij} \mathbf{R}_j. \quad (\text{A12})$$

and the site occupation matrix element is given by

$$n_{ab\mathbf{q}} = \sum_n [\mathbf{T}_{\mathbf{q}}]_{a+N_a, n+N_a} [\mathbf{T}_{\mathbf{q}}^*]_{n+N_a, b+N_a} n_{\text{B}}(\omega_{n, \mathbf{q}}), \quad (\text{A13})$$

where $n_{\text{B}}(\omega_{n, \mathbf{q}})$ is the Bose distribution and $\mathbf{T}_{\mathbf{q}}$ is the canonical matrix that transforms $\mathbf{a}_{\mathbf{q}}$ to a basis that (para)diagonalizes the Hamiltonian (20) [9, 13]

$$\boldsymbol{\alpha}_{\mathbf{q}} = \mathbf{T}_{\mathbf{q}} \mathbf{a}_{\mathbf{q}} \quad (\text{A14})$$

$$\boldsymbol{\alpha}_{\mathbf{q}} = \left[\alpha_{n, \mathbf{q}} \quad \alpha_{n, -\mathbf{q}}^\dagger \right]^T \quad n \in [1, N_a] \quad (\text{A15})$$

$$(\mathcal{H} - E_0) \alpha_{n, \mathbf{q}}^\dagger |0\rangle = \omega_{n, \mathbf{q}} \alpha_{n, \mathbf{q}}^\dagger |0\rangle, \quad (\text{A16})$$

where $E_0 = \mathcal{E}_0 + \mathcal{E}_{\text{K}}^0$ is the ground state energy. In this basis, the magnon number can be evaluated as

$$\Phi_a = \frac{1}{N} \sum_{\mathbf{q}} [\mathbf{T}_{\mathbf{q}} \langle \boldsymbol{\alpha}_{\mathbf{q}} \boldsymbol{\alpha}_{\mathbf{q}}^\dagger \rangle \mathbf{T}_{\mathbf{q}}^\dagger]_{a+N_a, a+N_a}, \quad (\text{A17})$$

$$\langle \boldsymbol{\alpha}_{\mathbf{q}} \boldsymbol{\alpha}_{\mathbf{q}}^\dagger \rangle = \begin{bmatrix} 1 + n_{\text{B}}(\omega_{n, \mathbf{q}}) & 0 \\ 0 & n_{\text{B}}(\omega_{n, \mathbf{q}}) \end{bmatrix}. \quad (\text{A18})$$

The procedure is described in more detail in Ref. [9].

Appendix B: Exchange contribution to the RPA Hamiltonian

The exchange contribution to the RPA Hamiltonian (36) is given by

$$\mathbf{H}_{\mathbf{q}}^{\text{RPA}} = \begin{bmatrix} -A_{ab\mathbf{q}}^{\text{RPA}} + C_{ab}^{\text{RPA}} & -B_{ab\mathbf{q}}^{\text{RPA}} \\ (B_{ab\mathbf{q}}^{\text{RPA}})^\dagger & (A_{ab-\mathbf{q}}^{\text{RPA}})^* - C_{ab} \end{bmatrix}, \quad (\text{B1})$$

$$A_{ab\mathbf{q}}^{\text{RPA}} = \frac{\langle S_a''z \rangle}{2} \mathbf{u}_a^T \mathbf{J}'_{ab\mathbf{q}} \mathbf{u}_b^*, \quad (\text{B2})$$

$$B_{ab\mathbf{q}}^{\text{RPA}} = \frac{\langle S_a''z \rangle}{2} \mathbf{u}_a^T \mathbf{J}'_{ab\mathbf{q}} \mathbf{u}_b, \quad (\text{B3})$$

$$C_{ab}^{\text{RPA}} = \delta_{ab} \sum_c \langle S_c''z \rangle \mathbf{v}_a^T \mathbf{J}'_{ac\mathbf{0}} \mathbf{v}_c, \quad (\text{B4})$$

with $\mathbf{J}'_{ab\mathbf{q}}$ defined as in Eq. (A11). This exchange Hamiltonian is used for both the RPA and RPA+CD approaches.

Appendix C: Magnon dispersion at zero temperature for Bravais lattices

In the case of Bravais lattices, the HP Hamiltonian at $T = 0$ can be expressed as

$$\mathbf{H}_{\mathbf{q}}^{\text{HP}} = -\frac{S}{2} \begin{bmatrix} X_{\mathbf{q}}^{\text{HP}} & Y_{\mathbf{q}}^{\text{HP}} \\ (Y_{\mathbf{q}}^{\text{HP}})^* & X_{\mathbf{q}}^{\text{HP}} \end{bmatrix}, \quad (\text{C1})$$

and the magnon energies can be obtained by the canonical transformation of this Hamiltonian:

$$\mathbf{T}_{\mathbf{q}}^{\dagger-1} \mathbf{H}_{\mathbf{q}}^{\text{HP}} \mathbf{T}_{\mathbf{q}}^{-1} = \frac{1}{2} \begin{bmatrix} \omega_{\mathbf{q}}^{\text{HP}} & 0 \\ 0 & \omega_{-\mathbf{q}}^{\text{HP}} \end{bmatrix}, \quad (\text{C2})$$

$$\omega_{\mathbf{q}}^{\text{HP}} = S \sqrt{X_{\mathbf{q}}^{\text{HP}2} - |Y_{\mathbf{q}}^{\text{HP}}|^2}. \quad (\text{C3})$$

The details of the required paradiagonalization and the construction of the transformation $\mathbf{T}_{\mathbf{q}}$ can be found in Refs. [9, 13, 44].

For the case of RPA, the magnon energies are easily obtained by diagonalizing the $T = 0$ Hamiltonian

$$\mathbf{H}_{\mathbf{q}}^{\text{RPA}} = S^{(0)} \begin{bmatrix} -X_{\mathbf{q}}^{\text{RPA}} & -Y_{\mathbf{q}}^{\text{RPA}} \\ (Y_{\mathbf{q}}^{\text{RPA}})^* & X_{\mathbf{q}}^{\text{RPA}} \end{bmatrix}, \quad (\text{C4})$$

$$\omega_{\mathbf{q}}^{\text{RPA}} = S^{(0)} \sqrt{X_{\mathbf{q}}^{\text{RPA}2} - |Y_{\mathbf{q}}^{\text{RPA}}|^2}. \quad (\text{C5})$$

If we exclude the contributions from Eq. (16) to $X_{\mathbf{q}}^{\text{HP}}$ and $Y_{\mathbf{q}}^{\text{HP}}$, the terms of order $\frac{1}{S}$ in Eqs. (27)-(28) are not present. In this case the dispersion relations predicted by HP and RPA at $T = 0$ are identical except the latter is renormalized by the saturation magnetization $S^{(0)}$ rather than the spin eigenvalue S .

Finally, for the case of RPA+CD, the magnon dispersion is given by

$$\omega_{\mathbf{q}}^{\text{RPA+CD}} = S^{(0)} \sqrt{X_{\mathbf{q}}^{\text{RPA+CD}2} - |Y_{\mathbf{q}}^{\text{RPA+CD}}|^2}, \quad (\text{C6})$$

$$X_{\mathbf{q}}^{\text{RPA+CD}} = \frac{\mathbf{u}^T \mathbf{J}'_{\mathbf{q}} \mathbf{u}^*}{2} - \mathbf{v}^T \mathbf{J}'_{\mathbf{q}} \mathbf{v} + (\mathbf{u}^T \mathbf{K} \mathbf{u}^* - 2\mathbf{v}^T \mathbf{K} \mathbf{v}) \Upsilon_{\text{CD}}, \quad (\text{C7})$$

$$Y_{\mathbf{q}}^{\text{RPA+CD}} = \frac{\mathbf{u}^T \mathbf{J}'_{\mathbf{q}} \mathbf{u}}{2} + \mathbf{u}^T \mathbf{K} \mathbf{u} \Upsilon_{\text{CD}}, \quad (\text{C8})$$

$$\Upsilon_{\text{CD}} = 1 - \frac{(S - \Phi^0)(1 + 2\Phi^0)}{2S^2}. \quad (\text{C9})$$

-
- [1] B. Huang, G. Clark, E. Navarro-Moratalla, D. R. Klein, R. Cheng, K. L. Seyler, D. Zhong, E. Schmidgall, M. A. McGuire, D. H. Cobden, W. Yao, D. Xiao, P. Jarillo-Herrero, and X. Xu, Layer-dependent ferromagnetism in a van der Waals crystal down to the monolayer limit, *Nature* **546**, 270 (2017), arXiv:1703.05892.
- [2] K. S. Burch, D. Mandrus, and J.-G. Park, Magnetism in two-dimensional van der waals materials, *Nature* **563**, 47 (2018).
- [3] Q. H. Wang, A. Bedoya-Pinto, M. Blei, A. H. Dismukes, A. Hamo, S. Jenkins, M. Koperski, Y. Liu, Q.-C. Sun, E. J. Telford, H. H. Kim, M. Augustin, U. Vool, J.-X. Yin, L. H. Li, A. Falin, C. R. Dean, F. Casanova, R. F. L. Evans, M. Chshiev, A. Mishchenko, C. Petrovic, R. He, L. Zhao, A. W. Tsien, B. D. Gerardot, M. Brotons-Gisbert, Z. Guguchia, X. Roy, S. Tongay, Z. Wang, M. Z. Hasan, J. Wrachtrup, A. Yacoby, A. Fert, S. Parkin, K. S. Novoselov, P. Dai, L. Balicas, and E. J. G. Santos, The magnetic genome of two-dimensional van der waals materials, *ACS Nano* **16**, 6960 (2022), pMID: 35442017, <https://doi.org/10.1021/acsnano.1c09150>.
- [4] N. D. Mermin and H. Wagner, Absence of ferromagnetism or antiferromagnetism in one- or two-dimensional isotropic heisenberg models, *Phys. Rev. Lett.* **17**, 1133 (1966).
- [5] D. Torelli and T. Olsen, Calculating critical temperatures for ferromagnetic order in two-dimensional materials, *2D Materials* **6**, 015028 (2018).
- [6] K. J. Strandburg, D. W. Hall, C. Liu, and S. D. Bader, Monte carlo simulations of the curie temperature of ultrathin ferromagnetic films, *Phys. Rev. B* **46**, 10818 (1992).
- [7] X. Lu, R. Fei, and L. Yang, Curie temperature of emerging two-dimensional magnetic structures, *Phys. Rev. B* **100**, 205409 (2019).
- [8] Y. Xue, Z. Shen, Z. Wu, and C. Song, Theoretical prediction of curie temperature in two-dimensional ferromagnetic monolayer, *Journal of Applied Physics* **132**, 053901 (2022).
- [9] V. Rajeev Pavizhakumari and T. Olsen, Predicting néel temperatures in helimagnetic materials, *Phys. Rev. B*

- 111, 184403 (2025).
- [10] T. Holstein and H. Primakoff, Field dependence of the intrinsic domain magnetization of a ferromagnet, *Phys. Rev.* **58**, 1098 (1940).
- [11] N. N. Bogolyubov and S. V. Tyablikov, Retarded and Advanced Green Functions in Statistical Physics, *Soviet Physics Doklady* **4**, 589 (1959).
- [12] R. A. Tahir-Kheli and D. ter Haar, Use of green functions in the theory of ferromagnetism. i. general discussion of the spin- s case, *Phys. Rev.* **127**, 88 (1962).
- [13] S. Toth and B. Lake, Linear spin wave theory for single- q incommensurate magnetic structures, *Journal of Physics: Condensed Matter* **27**, 166002 (2015).
- [14] H. B. Callen, Green function theory of ferromagnetism, *Phys. Rev.* **130**, 890 (1963).
- [15] V. Rajeev Pavizhakumari, T. Skovhus, and T. Olsen, Beyond the random phase approximation for calculating curie temperatures in ferromagnets: application to fe, ni, co and monolayer cri₃, *Journal of Physics: Condensed Matter* **37**, 115806 (2025).
- [16] P. Fröbrich and P. Kuntz, Many-body green's function theory of heisenberg films, *Physics Reports* **432**, 223 (2006).
- [17] F. B. Anderson and H. B. Callen, Statistical mechanics and field-induced phase transitions of the heisenberg antiferromagnet, *Phys. Rev.* **136**, A1068 (1964).
- [18] K. H. Lee and S. H. Liu, Green's-function method for antiferromagnetism, *Phys. Rev.* **159**, 390 (1967).
- [19] L. Chen, J.-H. Chung, M. B. Stone, A. I. Kolesnikov, B. Winn, V. O. Garlea, D. L. Abernathy, B. Gao, M. Augustin, E. J. G. Santos, and P. Dai, Magnetic field effect on topological spin excitations in cri₃, *Phys. Rev. X* **11**, 031047 (2021).
- [20] D. Soriano, M. I. Katsnelson, and J. Fernández-Rossier, Magnetic two-dimensional chromium trihalides: A theoretical perspective, *Nano Letters* **20**, 6225 (2020), pMID: 32787171, <https://doi.org/10.1021/acs.nanolett.0c02381>.
- [21] L. Chen, J.-H. Chung, B. Gao, T. Chen, M. B. Stone, A. I. Kolesnikov, Q. Huang, and P. Dai, Topological Spin Excitations in Honeycomb Ferromagnet CrI₃, *Physical Review X* **8**, 041028 (2018), arXiv:1807.11452.
- [22] A. Mook, K. Plekhanov, J. Klinovaja, and D. Loss, Interaction-stabilized topological magnon insulator in ferromagnets, *Phys. Rev. X* **11**, 021061 (2021).
- [23] S. K. Kim, H. Ochoa, R. Zarzuela, and Y. Tserkovnyak, Realization of the haldane-kane-mele model in a system of localized spins, *Phys. Rev. Lett.* **117**, 227201 (2016).
- [24] J. Cenker, B. Huang, N. Suri, P. Thijssen, A. Miller, T. Song, T. Taniguchi, K. Watanabe, M. A. McGuire, D. Xiao, and X. Xu, Direct observation of two-dimensional magnons in atomically thin cri₃, *Nature Physics* **17**, 20 (2021).
- [25] D. Lançon, R. A. Ewings, T. Guidi, F. Formisano, and A. R. Wildes, Magnetic exchange parameters and anisotropy of the quasi-two-dimensional antiferromagnet nips₃, *Phys. Rev. B* **98**, 134414 (2018).
- [26] P. A. Joy and S. Vasudevan, Magnetism in the layered transition-metal thiophosphates mps₃ (m=mn, fe, and ni), *Phys. Rev. B* **46**, 5425 (1992).
- [27] P. Jernberg, S. Bjarman, and R. Wäppling, Feps₃: A first-order phase transition in a "2d" ising antiferromagnet, *Journal of Magnetism and Magnetic Materials* **46**, 178 (1984).
- [28] A. R. Wildes, B. Roessli, B. Lebech, and K. W. Godfrey, Spin waves and the critical behaviour of the magnetization in mnps₃, *Journal of Physics: Condensed Matter* **10**, 6417 (1998).
- [29] A. R. Wildes, V. Simonet, E. Ressouche, G. J. McIntyre, M. Avdeev, E. Suard, S. A. J. Kimber, D. Lançon, G. Pepe, B. Moubaraki, and T. J. Hicks, Magnetic structure of the quasi-two-dimensional antiferromagnet nips₃, *Phys. Rev. B* **92**, 224408 (2015).
- [30] D. Lançon, H. C. Walker, E. Ressouche, B. Oulad-diaf, K. C. Rule, G. J. McIntyre, T. J. Hicks, H. M. Rønnow, and A. R. Wildes, Magnetic structure and magnon dynamics of the quasi-two-dimensional antiferromagnet feps₃, *Phys. Rev. B* **94**, 214407 (2016).
- [31] T. Olsen, Magnetic anisotropy and exchange interactions of two-dimensional feps₃, nips₃ and mnps₃ from first principles calculations, *Journal of Physics D: Applied Physics* **54**, 314001 (2021).
- [32] T. Y. Kim and C.-H. Park, Magnetic anisotropy and magnetic ordering of transition-metal phosphorus trisulfides, *Nano Letters* **21**, 10114 (2021), pMID: 34817186, <https://doi.org/10.1021/acs.nanolett.1c03992>.
- [33] M. Ovesen and T. Olsen, Giant orbital magnetization in two-dimensional materials, *2D Materials* **13**, 015001 (2025), publisher: IOP Publishing.
- [34] H. Katscher and H. Hahn, Über chalkogenidhalogenide des dreiwertigen chroms, *Naturwissenschaften* **53**, 361 (1966).
- [35] J. Beck, Über chalkogenidhalogenide des chroms synthese, kristallstruktur und magnetismus von chromsulfidbromid, crsbr, *Zeitschrift für anorganische und allgemeine Chemie* **585**, 157 (1990).
- [36] O. Göser, W. Paul, and H. Kahle, Magnetic properties of crsbr, *Journal of Magnetism and Magnetic Materials* **92**, 129 (1990).
- [37] K. Lee, A. H. Dismukes, E. J. Telford, R. A. Wiscons, J. Wang, X. Xu, C. Nuckolls, C. R. Dean, X. Roy, and X. Zhu, Magnetic order and symmetry in the 2d semiconductor crsbr, *Nano Letters* **21**, 3511 (2021), pMID: 33856213, <https://doi.org/10.1021/acs.nanolett.1c00219>.
- [38] E. J. Telford, A. H. Dismukes, K. Lee, M. Cheng, A. Wieteska, A. K. Bartholomew, Y.-S. Chen, X. Xu, A. N. Papaty, X. Zhu, C. R. Dean, and X. Roy, Layered antiferromagnetism induces large negative magnetoresistance in the van der waals semiconductor crsbr, *Advanced Materials* **32**, 2003240 (2020).
- [39] M. E. Ziebel, M. L. Feuer, J. Cox, X. Zhu, C. R. Dean, and X. Roy, Crsbr: An air-stable, two-dimensional magnetic semiconductor, *Nano Letters* **24**, 4319 (2024), pMID: 38567828, <https://doi.org/10.1021/acs.nanolett.4c00624>.
- [40] S. A. López-Paz, Z. Guguchia, V. Y. Pomjakushin, C. Witteveen, A. Cervellino, H. Luetkens, N. Casati, A. F. Morpurgo, and F. O. von Rohr, Dynamic magnetic crossover at the origin of the hidden-order in van der waals antiferromagnet crsbr, *Nature Communications* **13**, 4745 (2022).
- [41] Y. J. Bae, J. Wang, A. Scheie, J. Xu, D. G. Chica, G. M. Diederich, J. Cenker, M. E. Ziebel, Y. Bai, H. Ren, C. R. Dean, M. Delor, X. Xu, X. Roy, A. D. Kent, and X. Zhu, Exciton-coupled coherent magnons in a 2d semiconductor, *Nature* **609**, 282 (2022).
- [42] K. Yang, G. Wang, L. Liu, D. Lu, and H. Wu, Triaxial magnetic anisotropy in the two-dimensional ferro-

- magnetic semiconductor crsbr, *Phys. Rev. B* **104**, 144416 (2021).
- [43] A. Scheie, M. Ziebel, D. G. Chica, Y. J. Bae, X. Wang, A. I. Kolesnikov, X. Zhu, and X. Roy, Spin waves and magnetic exchange hamiltonian in crsbr, *Advanced Science* **9**, 2202467 (2022).
- [44] J. Colpa, Diagonalization of the quadratic boson hamiltonian, *Physica A: Statistical Mechanics and its Applications* **93**, 327 (1978).